

## Isolated and Interacting Galaxies : Simulations with GRAPE

E. Athanassoula

*Observatoire de Marseille, 2 place Le Verrier, 13248 Marseille cedex 04, France*

**Abstract.** I present  $N$ -body simulations of isolated and interacting galaxies, made on GRAPE machines. In particular I discuss the formation and evolution of  $N$ -body bars and compare their properties to those of bars in early-type and late-type galactic discs. I argue that the halo can help the bar grow, contrary to previous beliefs, by taking positive angular momentum from it via its resonant stars. I then focus on the interaction and subsequent merging of a barred disc galaxy with a spheroidal satellite. The evolution depends strongly on the mass (density) of the satellite and may lead to its destruction or to the destruction of the bar.

### 1. Introduction

GRAPE machines (Makino, these proceedings) have given a substantial boost to the study of galactic dynamics by making state of the art  $N$ -body simulations possible at a relatively low cost and by allowing a simulation environment which is much more flexible than that of supercomputing centers. Machines with even numbers, e.g. GRAPE-4 (Makino et al. 1997) and GRAPE-6 (Makino, these proceedings), have a very high accuracy arithmetic and calculate also the derivative of the force, thus allowing a more accurate integration scheme to follow the evolution, as well as calculations with little or no softening. In the field of galactic dynamics they are particularly suited for studying the nuclei of galaxies, the effect of black holes, as well as for problems where softening should be limited or avoided, or for other cases where high precision is necessary. Machines with odd numbers, as GRAPE-3 (Ebisuzaki et al. 1993) and GRAPE-5 (Kawai et al. 2000), have a more limited accuracy and do not provide the derivatives of the force. Nevertheless the accuracy of GRAPE-3 was shown to be amply sufficient for a large number of problems on galactic dynamics (e.g. Athanassoula et al. 1998) and GRAPE-5 is even more accurate (Kawai et al. 2000). They are thus very well suited for studies of the evolution of isolated and interacting galaxies, as well as of galaxy systems. They have therefore been widely used in these topics, as witnessed by the ever-increasing number of publications based on GRAPE simulations. The field of research thus covered is too broad to be usefully covered by a single review, so I will limit myself here to a few, largely unpublished, results obtained recently with the Marseille GRAPE systems. In sections 2 and 3 I will present results on the formation of bars and on the secular evolution of barred disc galaxies. In section 4 I will discuss the interaction and

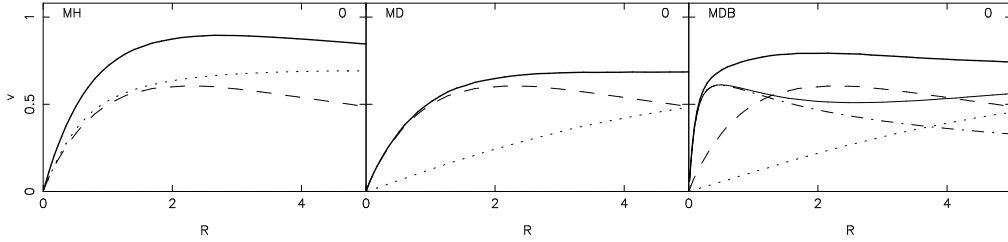


Figure 1. Circular velocity curves corresponding to the initial conditions of the three simulations discussed in section 2 (solid lines). The contribution of the disc, halo and bulge components are given by dashed, dotted and dot-dashed lines, respectively. The thin solid line in the right panel gives the total contribution of the two spherical components, halo and bulge. Here and in subsequent figures the names of the simulations are given in the upper left corner of each panel and the time in the upper right.

subsequent merging of a barred disc galaxy and a small elliptical companion. A few concluding remarks are given in section 5.

## 2. Formation and properties of bars in $N$ -body discs

Since the early seventies it is well known that galactic discs can be bar unstable (e.g. Miller, Prendergast & Quirk 1970; Hohl 1971). Nevertheless, the bar instability, and in particular its origin and its effect on galaxy evolution, are still not well understood (e.g. Sellwood 2000). Let me add here some new elements to this discussion with the help of three fully self-consistent simulations, run on the Marseille GRAPE-5 systems. In this section I will introduce the simulations and discuss the morphology of the ensuing  $N$ -body bar. In the next section I will touch on the origin of the instability and in particular on the role of the halo.

In all three simulations described here the disc component is an exponential disc of unit scale length and unit mass. The halo component is initially thermalised, spherical and non-rotating, and has a total mass five times that of the disc. The first two simulations have haloes of very different central concentrations. This can be seen in Fig. 1, which shows the initial circular velocity curves, together with the contribution of each component separately. We will call the simulation with the concentrated halo MH, for massive halo, since the halo is somewhat more massive than the disc in the inner parts, and the second one MD, for massive disc, since now it is the disc component that dominates in the inner parts. The initial conditions of the third simulation are identical to those of the second one, except that it has also a Plummer sphere bulge of mass 0.6 and radius 0.4. We will hereafter refer to it as MDB, for massive disc with bulge. The number of particles is of the order of  $1.2 \times 10^6$ . These three initial conditions are very similar to those described in Athanassoula & Misiriotis (2002, hereafter AM), except that the disc here is initially somewhat thinner. A reasonable calibration (AM) gives that  $t = 500$  corresponds to  $7 \times 10^9$  years.

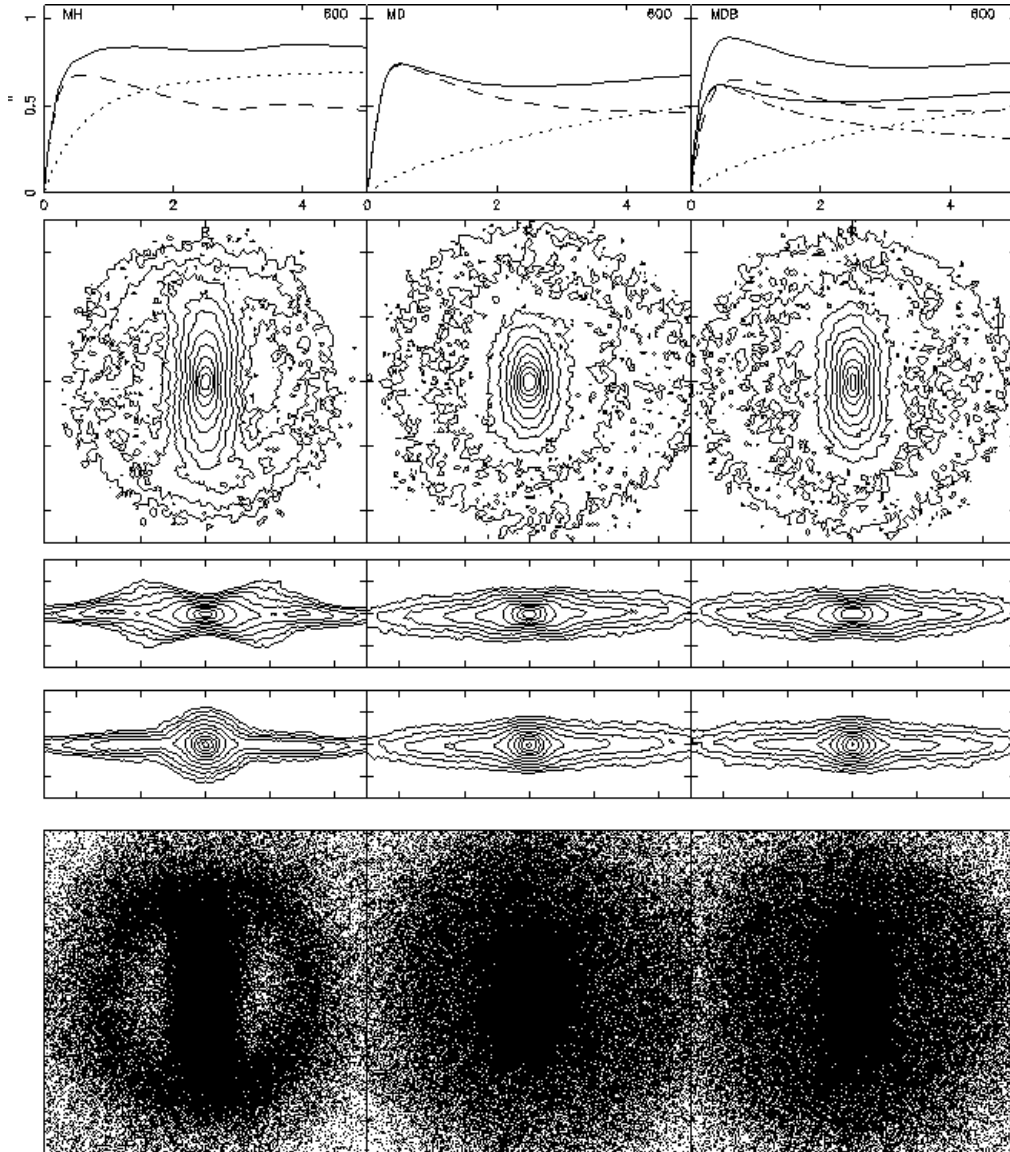


Figure 2. Our three fiducial models at time 600. The three upper panels show the circular velocity curves, and their layout is the same as for Fig. 1. The next three rows of panels show isodensity contours of the disc component, seen face-on (second row), and edge-on with the bar seen side-on (third row) and end-on (fourth row). The fifth row of panels shows the dot-plots of the face-on distributions. The size of the square box for the second and fifth row of panels is 10 initial disc scale lengths, and all panels, except for the upper row, have the same linear scale.

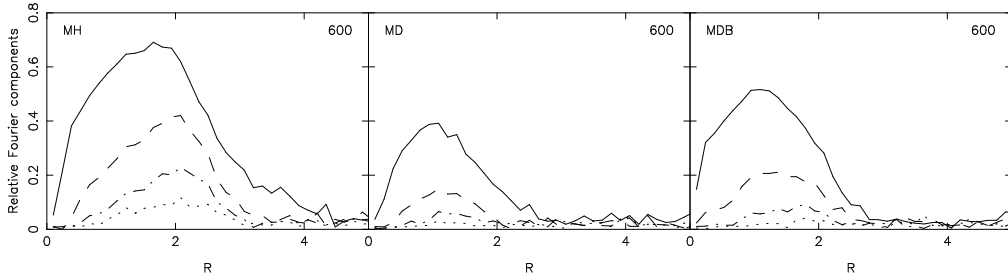


Figure 3. Relative Fourier components of the face-on density distribution. The  $m = 2, 4, 6$  and  $8$  components are plotted with a solid, dashed, dot-dashed and dotted line respectively.

Different values, however, can be obtained for different scalings of the disc mass and scale length.

We let these simulations evolve up to time 900. In all three cases a bar forms, but its properties are different, as witnessed in Fig. 2, which shows results for time 600. The upper panels show the circular velocity curves. Comparing them with the initial ones, we see that in all three cases the disc component is considerably more centrally concentrated than at time  $t = 0$ . In model MD the difference is only quantitative, since the disc dominates in the inner parts both at  $t = 0$  and at  $t = 600$ , while for model MH the difference is qualitative, since at  $t = 600$  the disc dominates in the inner parts, contrary to what was the case initially.

We note very large morphological differences between models MH and MD, model MDB being intermediate. Thus the bar in model MH is stronger, longer and more rectangular-like than in model MD. It also has a massive ring surrounding the bar, whose diameter is roughly equal to the bar major axis, as is the case for inner rings in real galaxies (Kormendy 1979, Buta 1986). It is somewhat elongated along the bar, in good agreement with observations of inner rings (Buta 1995). Model MDB has a bar of intermediate length and shape.

Let us now compare the properties of  $N$ -body bars with those of bars in early and late type galaxies. Bars in early type galaxies are longer than those in late type ones (Elmegreen & Elmegreen 1985) and have rectangular-like isophotes (Athanassoula et al. 1990), as the bar in model MH. Furthermore, the bar in MH-type simulations often has ansae, a feature seen only in early type barred galaxies (good examples are shown on page 42 of the Hubble Atlas of Galaxies, Sandage 1961). Thus the bar in MH-type models can be compared to a bar in an early type galaxy, while that in MD-type models with a late type.

The edge-on views of the three models are also quite different. Model MD shows a boxy shape when viewed side-on, while model MH has a strong peanut. Such shapes are indeed observed in many edge-on galaxies and are linked to the existence of a bar in the disc (Kuijken & Merrifield 1995, Bureau & Athanassoula 1999, Athanassoula & Bureau 1999).

Fig. 3 shows the relative  $m = 2, 4, 6$  and  $8$  Fourier components of the face-on density, for the three models. We note that they are much larger for model MH, as could be expected since the bar is stronger. Let me stress that

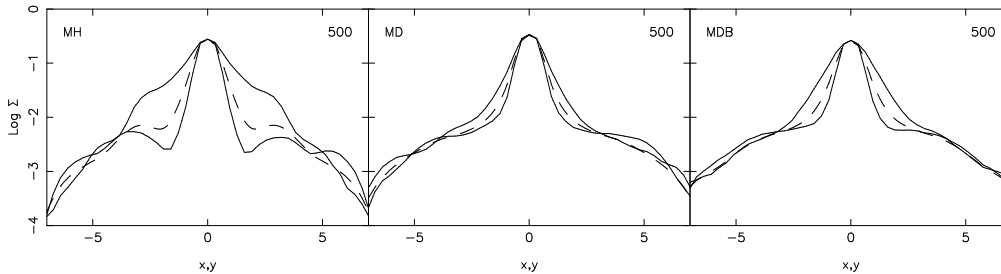


Figure 4. Projected surface density of the disc component viewed face-on. The solid lines correspond to cuts along the major and minor axes of the bar. The dashed line is obtained by azimuthal averaging.

the  $m = 6$  and  $8$  components are in the noise for model MD, while they are important for model MH. Note also that the  $m = 4$  and  $6$  components in model MH have relative amplitudes of the same order as the  $m = 2$  in model MD. Such Fourier components have also been calculated for real barred galaxies. In his review, Ohta (1996) describes them both for early and for late type galaxies and his descriptions fit well models MH and MD respectively. Thus he stresses that for early type galaxies the relative even Fourier components are large and the higher  $m$  components are important. On the contrary for late type bars all relative Fourier components have lower amplitude, while the high  $m$  components are negligible (cf. his Fig. 2).

Let us now try and compare the results of the  $N$ -body simulations with photometric results. For this we view the galaxy face-on and obtain the projected density profile along the directions of the bar major and minor axes (Fig. 4). We note that for model MH the profile along the bar major axis has flat parts on either side of the center, followed by steep drops at the ends of the bar. The picture is totally different for model MD, where the profile drops clearly all through the bar region, and there is no clear change of slope at the end of the bar. Observers have made similar cuts for many barred galaxies. Elmegreen & Elmegreen (1985) classify these profiles in two types : *flat*, which are reminiscent of the profile of model MH, and *exponential*, which are similar to that of model MD. They stress that flat profiles are found in early type galaxies, while exponential ones mainly in late types. Similar conclusions were reached by Ohta, Hamabe & Wakamatsu (1990), Ohta (1996), etc. Thus again model MH resembles bars in early type galaxies and model MD late type ones.

Let us repeat the exercise, now viewing the galaxy edge-on and the bar side-on. The results are shown in Fig. 5. For model MH the cuts at high  $z$  values show a minimum at the center, followed by two maxima, one on either side, and then a steep drop. This is the clear signature of a peanut. Similar features, but of *much* lower amplitude, can also be seen for model MD, revealing the existence of a weak peanut or a boxy feature. For model MH, the cuts at  $z = 0$  show a ledge on either side of the nucleus, followed by a relatively sharp drop. Lütticke et al. (2000) have made similar profiles for a large number of edge-on galaxies and their profiles are in good agreement with those of Fig. 5. They also find a correlation, in the sense that it is the strongest peanuts that have the most pronounced ledges, i.e. the strongest bars. This could be predicted from

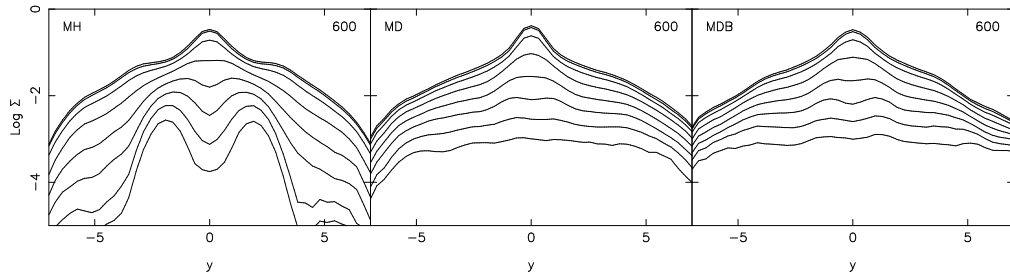


Figure 5. Projected surface density of the disc component viewed edge-on, with the bar seen side-on. The various profiles are obtained from cuts at various distances from the equatorial plane. The top-most one is for  $z = 0$  and the rest are spaced by  $\Delta z = 0.2$  apart. Thus the lower-most one corresponds to  $z = 1.4$ .

the simulations, both those described here, and others with somewhat different sets of initial parameters. If models of type MH are indeed associated with early type galaxies, then the simulations predict that the strongest peanuts will form in early types. This is unfortunately difficult to verify since it is difficult to find the morphological type of an edge-on disc galaxy.

Fig. 6 shows the velocity field of the models seen edge-on. We note that when the viewing angle is along the bar minor axis, i.e. when the bar is viewed side-on, the velocities within the bar/peanut region do not change much with distance from the equatorial plane. This behaviour is often termed ‘cylindrical rotation’ and was observed for many peanut galaxies (e.g. NGC 4565, Kormendy & Illingworth 1982; NGC 3079, Shaw, Wilkinson & Carter 1993; NGC 128, D’Onofrio et al. 1999).

In all the above comparisons model MDB is intermediate between models MH and MD. This holds for the length of the bar and the shape of its face-on isophotes, as well as for its Fourier components and the strength of its peanut. For this model we also analysed the form of the bulge. This starts initially as spherical but evolves to oblate, with its shortest dimension perpendicular to the equatorial plane. The departures from sphericity are strongest for the innermost isophotes, which are also triaxial. Here we find axial ratios of the order of 0.7 and 0.75. At intermediate radii we find ratios of the order of 0.9 and 0.8, while in the outer bulge parts the form of the isophotes approaches a sphere.

It is also worth adding a few words about the inner parts of the bar/disc component in model MH. If the bar is seen edge-on and the bar end-on (Fig. 2, panel in fourth row and left column), then the bar presents a structure which could be easily mistaken for an intermediate size bulge in an edge-on disc galaxy. This impression is reinforced if we look at the projected density profiles of the  $N$ -body system. Such ‘bulges’ could be erroneously included in observational studies of bulges in edge-on disc systems.

Summarising this section I note that the results of the  $N$ -body simulations reproduce well the morphology, the photometry and the kinematics of barred galaxies. They also produce strong arguments linking early type barred galaxies with simulations in which the halo is *initially* centrally concentrated and late type galaxies with simulations where the center part is *initially* disc dominated.

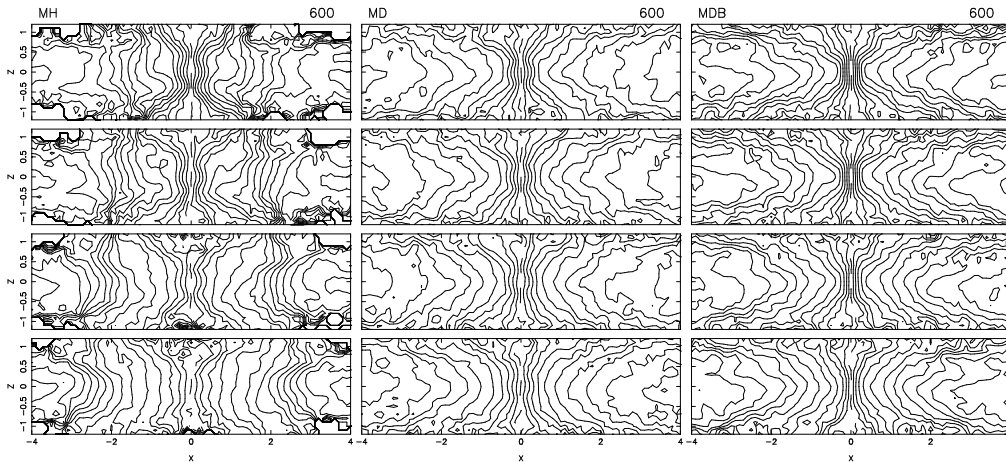


Figure 6. Velocity field of the disc component seen edge-on. In the upper panels the bar is seen end-on and in the lower ones side-on. The second and third row of panels are for intermediate viewing angles, at 30 and 60 degrees from the bar major axis, respectively.

### 3. The role of the halo

In the above we saw that the strongest bar formed in the case where the halo contribution in the disc region is initially the strongest. In order to understand this I froze the potential of both models MH and MD at time  $t = 500$  and calculated orbits of 200 000 particles chosen at random from the simulation particles – half taken from the disc and half from the halo –. For each orbit I calculated the basic frequencies  $\Omega$ ,  $\kappa$  and  $\kappa_z$ , i.e. the angular, epicyclic and vertical frequencies. This is not always a straightforward calculation. Although the results for of the order of 10% of the particles are not very reliable, in particular for  $\Omega$ , the remainder are precise enough to warrant discussion.

Fig. 7 shows the number density of particles/orbits that have a given value of  $(\Omega - \Omega_p)/\kappa$  as a function of this ratio, for run MH. We note that the distribution is far from homogeneous and that there are large peaks at the main resonances. This could have been expected for the disc particles, although the sharpness and the amplitude of the resonance peaks is worth noting. What is more novel and exciting, however, is the existence and the amplitude of the resonant peaks in the halo population, which has often been considered as a non- or little-responsive component. For the disc particles the highest peak is at the Inner Lindblad resonance (ILR), followed by corotation (CR) and inner Ultra-harmonic or 1:4 resonances. For the halo the highest peak is at CR, followed by the outer Lindblad resonance (OLR) and then the ILR. The amplitude of the peaks varies with time, but also from one simulation to another, as will be discussed in detail elsewhere.

Disc stars at resonances can give or take angular momentum, and thus contribute to the evolution of the system. Stars at ILR emit angular momentum, while stars at CR or OLR absorb it (Lynden-Bell & Kalnajs 1972). The resonant halo stars generally absorb angular momentum (Tremaine & Weinberg 1984).

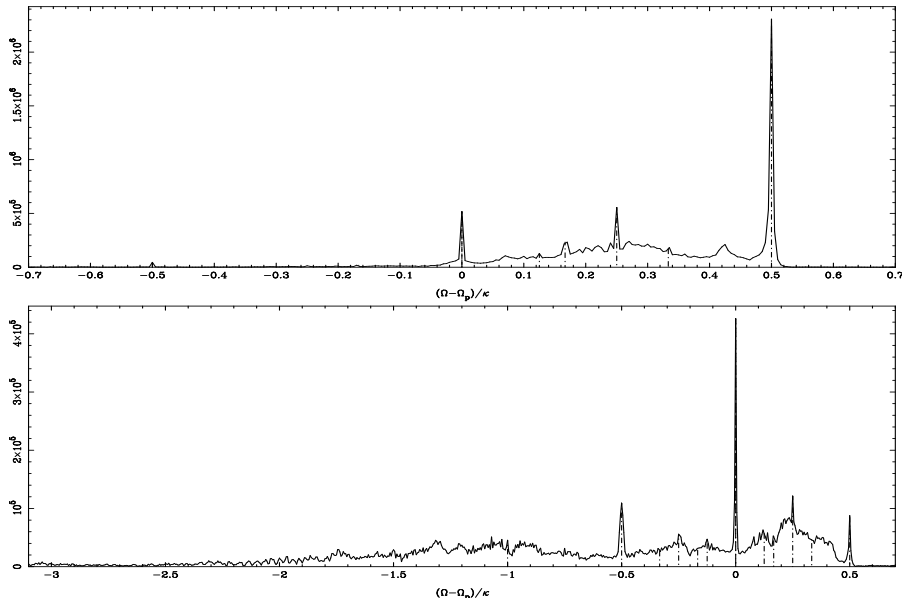


Figure 7. Number density of particles as a function of the frequency ratio  $(\Omega - \Omega_p)/\kappa$  for model MH and time 500. The upper panel corresponds to the disc particles and the lower one to the halo ones. The dot-dashed vertical lines mark the positions of the main resonances.

Thus, together with the disc stars at CR and OLR, they will destabilise the bar and induce it to increase its amplitude, since the bar has negative energy and angular momentum. This can also be seen in a simpler way if we calculate the angular momentum of the two components (not plotted here). A more explicit and quantitative treatment of this exchange will be given elsewhere, but the short discussion above can give some insight as to why a halo may help the bar grow stronger, instead of stabilising it.

#### 4. Merging of a barred galaxy with a satellite

GRAPE is particularly useful for simulations of interacting systems, since its force calculation does not depend on geometry, contrary to grid or expansion methods. The simulations I will present here describe the interaction and subsequent merging of a barred disc galaxy with its spherical satellite. The target galaxy is composed of a disc and a halo component with a mass ratio  $M_h/M_d = 0.54$ . The satellite is modeled with a Plummer sphere of mass  $M_s$  and is initially placed near the edge of the halo in a direct near-circular orbit in the disc plane. We consider two different companion masses, one equal to the mass of the disc and the other one tenth of that. Since the scale lengths are the same in the two cases, the ratio of masses reflects also the ratio of densities.

Due to dynamical friction, the companion spirals inwards and reaches the center of the target galaxy. The rate at which it does so depends heavily on

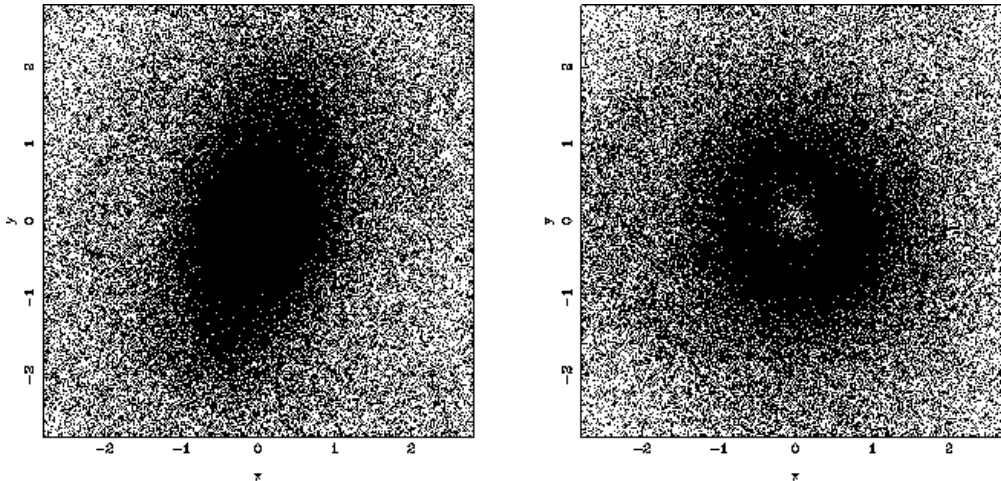


Figure 8. Face-on view of the disc particles at the beginning of the simulation (left panel) and after the merging with the high mass companion (right panel). As a result of the merging the initial bar has disappeared and a low density region has formed in the central parts, occupied by the companion particles (not plotted here).

its mass. Thus the high mass companion reaches the center in one third of the time taken by the low mass companion. As a result of this evolution the target disc thickens, but also expands, so that its aspect ratio, when seen edge-on, does not change much, staying that of a disc (cf. Fig. 4 of Athanassoula 1996). The companion, occupying the central region, forms a bulge, or contributes to one (cf. also Walker, Mihos & Hernquist 1996). Its shape is oblate and it has lost only a small fraction of its initial mass.

We thus have an evolution of the target galaxy from late to early type. If the plane of the initial companion orbit is at an angle to that of the disc, then the target disc still thickens and expands, but it also tilts, so that the final equatorial plane is, for the case of the massive companion, not far from that of the companion's initial orbital plane. For the low mass companion it tilts much less, but still the tilt is noticeable. The energy of the vertical motion of the companion, due to the tilt, is transformed mainly to an organised motion of the disc particles, rather than to an increase of the vertical component of the velocity dispersion, so that the disc is not excessively thickened (cf. also Athanassoula 1996, Huang & Carlberg 1997).

The high mass companion exerts a strong perturbation on the bar, which of course becomes stronger as the companion approaches the central regions of the target galaxy. Particles are drawn from the bar in the direction of the companion, so that the bar is progressively emptied, loses its identity and by the time the companion reaches the center the bar has wrapped around it. Thus after the merging the target is a non-barred galaxy and its disc projected surface density has a minimum in the central region (left panel of Fig. 8), which is now occupied by the companion (cf. Fig. 2 of Athanassoula 1996).

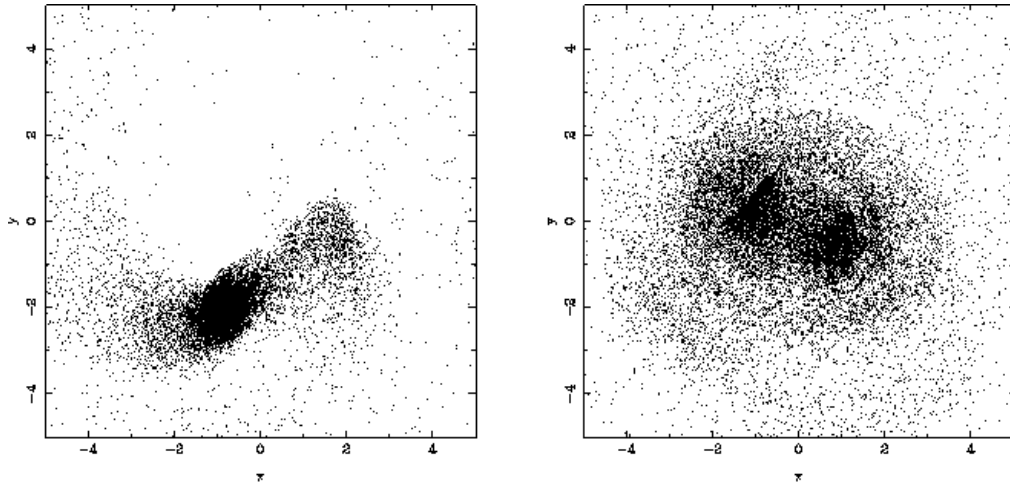


Figure 9. Fate of the low mass companion during the merging. The companion loses particles preferentially from the direction of its motion and the diametrically opposite direction, and becomes elongated along the orbit (left panel). The companion is thus disrupted and, after the merging is completed, its particles orbit around the bar of the target galaxy, extending and elongating it (right panel).

The evolution is quite different in the case with the low mass companion. Now it is the companion that gets most perturbed, particularly after it has reached the disc region. It loses particles, not uniformly from all its surface, but from two preferred directions, one in the direction of the motion and the other opposite to it. As it does so its mass decreases and it also loses its initial spherical shape and becomes strongly elongated in the direction of the orbital motion (left panel of Fig. 9). When it reaches the bar region, the companion loses particles at a yet higher rate, until it disintegrates. Its particles then orbit around the bar in elongated orbits, staying longer near the bar major axis. At any moment there is a concentration of companion particles around the two opposite ends of the bar, thus extending and lengthening it (right panel of Fig. 9). These concentrations are not transient.

The in-falling satellite perturbs also the halo component. The most massive companion induces a considerable spin in the direction of the initial rotation of the companion. Furthermore the halo velocity dispersion increases locally at the location of the companion. This creates a local maximum of the velocity dispersion, which moves inwards with the satellite. The velocity dispersion after the companion has reached the center is larger than the initial one, particularly in the central parts. The heating of the disc has been examined by Walker et al. (1996), Huang & Carlberg (1997) and Velázquez & White (1999).

## 5. Summary

In the above I presented results of simulations made with the Marseille GRAPE systems. I started with simulations of the formation and evolution of a bar in

an isolated disc galaxy. These show that strong bars can form in systems with a sizeable halo component within the disc region. I find very good agreement between the properties of the  $N$ -body bars and those of bars in galaxies. In particular I presented arguments that link  $N$ -body bars that grew in an environment with a considerable halo component with early type bars, and bars growing in a disc-dominated environment with late type bars. Such simulations stress the role of the halo in the development of the bar instability and show that the halo can stimulate bar formation, contrary to the common belief that it will always quench it. The reason is that the halo responds to the bar and a considerable fraction of its particles are in resonance with it. This of course would have been missed by simulations treating the halo as a rigid component.

I then discussed the interaction and subsequent merging of a barred disc galaxy with its spherical satellite. If the satellite has high mass (density), then it will spiral rapidly towards the center of the disc, destroy the bar and occupy the center of the target, thus forming a bulge, or contributing to one. Such interactions will cause evolution along the Hubble sequence, from late to early type discs. During this process the disc thickens considerably, but also expands, so that its final shape is still that of a disc, albeit somewhat thicker than the initial one. If the companion has low mass (density), then it will get disrupted as it spirals inwards towards the center of the target. If the orbit of the companion is initially at an angle with the plane of the disc, then the disc tilts but is not destroyed. In the case of the high mass (density) companion, the tilt angle is not far from that of the plane of the initial orbit of the companion.

The above results, and many others not shown here, argue that GRAPE is an ideal tool for simulations of galaxies and galaxy systems. In all the above simulations the number of particles was of the order of a million, or more than that. This is now a standard number for most of our GRAPE simulations. GRAPE can of course handle considerably larger numbers, provided its front end has a sufficient memory, and we have used such numbers whenever necessary.

GRAPE boards permit fast and accurate calculations of the gravitational potential and forces, and are not limited by the specific geometry of the particle distribution. Their price is a very small fraction of that of supercomputers. Both high precision direct summation codes and tree codes have been developed for them. They offer a flexible simulation environment. They are thus ideally suited for small research groups ready to invest themselves in the GRAPE approach. The close collaboration between the members of the international community of GRAPE users contributes further to the success of these machines.

**Acknowledgments.** First and foremost I would like to thank the Tokyo group – headed initially by D. Sugimoto and later by J. Makino – for developing the GRAPE systems, without which the simulations presented here would not have been possible. I would like to thank Albert Bosma for many discussions on barred galaxies and A. Misiriotis for his collaboration on the software calculating the orbital frequencies. I would also like to thank the IGRAP, the Region PACA, the INSU/CNRS and the University of Aix-Marseille I for funds to develop our GRAPE computing facilities.

**References**

- Athanassoula, E. 1996, in *Barred Galaxies and Circumnuclear Activity*, ed. Aa. Sandqvist, P. O. Lindblad, (Springer), 59
- Athanassoula, E., Bosma, A., Lambert, J. C., & Makino, J. 1998, *MNRAS*, 293, 369
- Athanassoula, E., & Bureau, M. 1999, *ApJ*, 522, 699
- Athanassoula, E., & Misiriotis, A. 2002, *MNRAS*, in press and astro-ph/0111449 (AM)
- Athanassoula, E., Morin, S., Wozniak, H., Puy, D., Pierce, M., Lombard, J. & Bosma, A. 1990, *MNRAS*, 293, 369
- Bureau, M. & Athanassoula, E. 1999, *ApJ*, 522, 686
- Buta, R. 1986, *ApJS*, 61, 609
- Buta, R. 1995, *ApJS*, 96, 39
- D’Onofrio, M., Capaccioli, M., Merluzzi, P., Zaggia, S., Boulesteix, J. 1999, *A&AS*, 134, 437
- Ebisuzaki, T., Makino, J., Fukushige, T., Taiji, M., Sugimoto, D., Ito, T., Okumura, S. 1993 *PASJ*, 45, 269
- Elmegreen, B. G. & Elmegreen D. M. 1985, *ApJ*, 288, 438
- Hohl, F. 1971, *ApJ*, 168, 343
- Huang, G., & Carlberg, R. G. 1997, *ApJ*, 480, 503
- Kawai, A., Fukushige, T., Makino, J., & Taiji, M. 2000, *PASJ*, 52, 659
- Kormendy, J. 1979, *ApJ*, 227, 714
- Kormendy, J. & Illingworth, G. 1982, *ApJ*, 256, 460
- Kuijken, K. & Merrifield, M. R. 1995, *ApJ*, 443, L13
- Lütticke, R., Dettmar, R.-J., & Pohlen, M. 2000, *A&A*, 362, 435
- Lynden-Bell, D., & Kalnajs, A. J. 1972, *MNRAS*, 157, 1
- Makino, J., Taiji, M., Ebisuzaki, T., & Sugimoto, D. 1997, *ApJ*, 480, 432
- Miller, R. H., Prendergast, K. H., & Quirk 1970, *ApJ*, 161, 903
- Ohta, K. 1996, in *ASP conference Series Vol 91, Barred Galaxies*, eds. R. Buta, D. A. Crocker, B. G. Elmegreen, 37
- Ohta, K., Hamabe, M. & Wakamatsu, K. 1990, *ApJ*, 357, 71
- Sandage, A. 1961, *The Hubble Atlas of Galaxies*, (Washington : Carnegie Institution Publications)
- Sellwood, J. A. 2000, in *ASP conference Series Vol 197, XVth IAP Meeting, Dynamics of Galaxies: From the Early Universe to the Present*, eds. F. Combes, G. A. Mamon & V. Charmandaris, 3
- Shaw, M., Wilkinson, A., & Carter, D. 1993, *A&A*, 268, 511
- Tremaine, S., & Weinberg, M. D. 1984, *MNRAS*, 209, 729
- Velázquez H., & White, S. D. M. 1999, *MNRAS*, 304, 254
- Walker, I. R., Mihos, J. C., & Hernquist, L. 1996, *ApJ*, 460, 121